1	Wireless monitoring of respiration with EEG reveals relationships between
2	respiration, behaviour and brain activity in freely moving mice
3	
4	Debanjan Dasgupta ^{1,2,3,4*} , Deborah Schneider-Luftman ¹ , Andreas T. Schaefer ^{1,2*} ,
5	Julia J. Harris ^{1,2,4*}
6	
7	¹ The Francis Crick Institute, Sensory Circuits and Neurotechnology Laboratory, London, Uk
8	² Department of Neuroscience, Physiology & Pharmacology, University College London, Uk
9	³ UK Dementia Research Institute, UCL
10	⁴ These authors contributed equally
11	*Correspondence should be addressed to debanjan.dasgupta@crick.ac.uk ,
12	andreas.schaefer@crick.ac.uk, or julia.harris@crick.ac.uk
13	
14	
15	
16	

ABSTRACT

17

18

19

20

21

22

23

24

25

26

27

28

29

30

31

32

33

34

35

36 37

Active sampling in the olfactory domain is an important aspect of mouse behaviour, and there is increasing evidence that respiration-entrained neural activity outside of the olfactory system sets an important global brain rhythm. It is therefore important to accurately measure breathing during natural behaviours. We develop a new approach to do this in freely moving animals, by implanting a telemetry-based pressure sensor into the right jugular vein, which allows for wireless monitoring of thoracic pressure. After verifying this technique against standard head-fixed respiration measurements, we combined it with EEG and EMG recording and used evolving partial coherence analysis to investigate the relationship between respiration and brain activity across a range of experiments in which the mice could move freely. During voluntary exploration of odours and objects, we found that the association between respiration and cortical delta and theta rhythms decreased, while the association between respiration and cortical alpha rhythm increased. During sleep, however, the presentation of an odour was able to cause a transient increase in sniffing without changing dominant sleep rhythms (delta and theta) in the cortex. Our data align with the emerging idea that the respiration rhythm could act as a synchronising scaffold for specific brain rhythms during wakefulness and exploration, but suggest that respiratory changes are less able to impact brain activity during sleep. Combining wireless respiration monitoring with different types of brain recording across a variety of behaviours will further increase our understanding of the important links between active sampling, passive respiration, and neural activity.

39 40

38

Key Words: Respiration, EEG, Exploration, Sleep

41 42

43

44

45 46

47

48

49

New and Noteworthy

Animals can alter their respiration rate to actively sample their environment, and increasing evidence suggests that neurons across the brain align their firing to this changing rhythm. We developed a new approach to measure sniffing in freely moving mice whilst simultaneously recording brain activity, and uncovered how specific cortical rhythms changed their coherence with respiration rhythm during natural behaviours and across arousal states.

INTRODUCTION

50

51 52

53

54

55

56

57

58 59

60

61

62

63 64

65

66

67

68

69 70

71

72

73

74

75

76

77

78

79

80

81

82

83

Active sampling plays a crucial role in sensory processing (1), particularly within the sense of olfaction (2; 3; 4; 5; 6,7; 8). Olfactory sampling is governed by the respiration rhythm, and many mammals display a huge repertoire of "sniffing" behaviours which dynamically alter their respiration rate (9; 10; 11; 6,7). In turn, respiration-entrained neuronal firing patterns are increasingly being observed across brain regions outside of the olfactory system, including the hippocampus, neocortex and limbic system (reviewed in 12). Accumulating evidence has led to the hypothesis that breathing sets a global brain rhythm to actively coordinate neuronal communication across distant brain regions (13; 14; 15) which may contribute to learning and memory (16). It is now being discovered that the alignment of different neural activity patterns to this respiration rhythm can change with the arousal state and behaviour of the animal (17; 18; 19; 20; 21; 22). During exploration, respiratory rhythms overlap in frequency with the hippocampal theta rhythm (23) and confusion may therefore arise in the absence of knowledge about the animal's breathing. Accurately measuring sniffing is therefore critical not only in the fields of respiratory physiology and olfaction, but also in the context of animal behaviour and neural processing more generally.

Over the years, different strategies have been developed to monitor respiration (24), including whole-body plethysmography (25; 26–28; monitoring chest distension using piezoelectric bands (29,30); thermal imaging of nostrils (31); and monitoring changes in nasal air flow (29,32-35), pressure (36; 6,36-38), or temperature (39–44). However, these methods all require specific recording conditions or tethering, making it difficult to measure respiration during natural behaviours or in combination with other recording techniques. Recently, an innovative approach was developed, which has the potential to overcome this challenge. Specifically, a wireless pressure sensor was threaded alongside the oesophagus and implanted into the thoracic cavity, where it could detect thoracic pressure changes that directly reflect respiration (37). This approach was applied in awake, freely moving animals, allowing respiration to be monitored in a natural environment and during behavioural tasks.

In the current study, we present a new surgical approach to implant a wireless thoracic pressure sensor into the jugular vein, and verify the thoracic pressure signal against a head-fixed flow-sensor recording. Probe insertion into the jugular vein,

rather than alongside the oesophagus wall (37) simplified the postoperative care, with no requirement for a change to liquid-based diet. This surgical approach is thus more suitable for typical learning assays where water restriction is required for training. We then use this technique in conjunction with implanted EEG and EMG electrodes to measure brain activity in freely moving mice. We examined respiration pattern changes as mice voluntarily explored novel objects, novel odours and food odours, and also across different arousal states, while simultaneously examining the relationship between respiration and cortical rhythms. Gaining insight into how respiration relates to brain activity and behaviour will provide new opportunities to understand how animals process the world around them and interact with their environment.

95

84

85

86 87

88 89

90

91

92

93

94

MATERIALS AND METHODS

97

98

99

100

101

102

103

104

105

106

107

108

109

110

111 112

113

114

115

116 117

118

119

120

121

122

123

124 125

126 127

128

129

130

Implantation of thoracic pressure sensor in right jugular vein

All animal procedures performed in this study were regulated and approved by the Institutional Animal Welfare Ethical Review Panel and the UK government (Home Office) under license PA2F6DA12. All the surgeries and behavioural assays were performed on male C57/BI6 mice.

Thoracic pressure sensors (Stellar implantable transmitter device, 10X normal gain, E-430001-IMP-22, TSE systems, Germany) were implanted in the right jugular vein in mice. 6-8 weeks old animals were put in individual cages 2 days before surgery to ensure acclimatization and proper intake of drugs orally. On the day prior to the surgery, 0.2ml of egg custard (Cow & Gate) + 0.2ml oral Metacam suspension was given in addition to freely available food. On the day of surgery, the animal was weighed and anesthetized using Fentanyl (0.05mg/kg) + Midazolam (5mg/kg) + Medetomidine (0.5mg/kg), delivered ip. Further, for analgesia Meloxicam (10mg/kg) + Buprenorphine (0.1mg/kg) was administered subcutaneously. The animals were then placed on a heatpad (DC Temperature Controller, FHC, USA) controlled by a rectally inserted temperature sensor. Body temperature was continuously monitored and maintained at 37 ± 0.5 °C. The probes consisting of two parts, a transmitter (2cm X 1cm X 0.3cm) and a catheter (5cm long and ~0.4mm diameter), were implanted using aseptic surgery techniques. The skin on the right of the neck's midline was shaved and disinfected with 25% (v/v) chlorhexidine. Next, a ~2 cm skin incision was made and using blunt tools a subcutaneous tunnel was created underneath the right arm up to the back of the animal. Pre-sterilised saline solution was used to irrigate the wound regularly. The transmitter was pushed through this tunnel up to the back of the animal (Fig. 1B) while keeping the sensor end out of the wound. Next, post isolation of the right jugular vein, a knot was tied on the dorsalmost part of the isolated section of the vein using non-soluble surgical sutures (Fig. 1C). A small incision was made on the vein surface to insert the sensor tip of the catheter (Fig. 1D). During the process of insertion of the sensor tip (Fig. 1E), the pressure signal was continuously monitored to identify the best spot for placement. Upon reaching the best spot, a knot was firmly tied around the vein enclosing the catheter (Fig. 1F). The remaining suture thread from the dorsal knot was also used to make a knot around the catheter for extra stability of the placed sensor. Finally, the wound was closed using 6-0 silk suture and a reverse-cutting needle. The

animal was recovered in a heated chamber after injecting 1.2mg/kg Naloxone + 0.5mg/kg Flumazenil + 2.5mg/kg Atipamezole (ip). Sterile saline (0.2 ml) was injected subcutaneously for faster recovery. The animals were monitored and their bodyweights were recorded regularly at least for the next 10 days post-surgery.

For the head-fixed recordings, a subset of animals also underwent a headfixation implant attachment in the same surgery. Briefly, a custom-made headfixation implant was glued to the skull with a medical grade superglue (Vetbond, 3M, Maplewood MN, USA). Further, dental cement (Palladur, Heraeus Kulzer GmbH, Hanau, Germany) was applied around the base of the implant to strengthen the fixation.

Post-surgery the animals were allowed at least a week to recover from the surgery and to get back to their pre-surgery body weights before being used for experiments.

EEG and EMG electrode implantation

131

132 133

134

135

136

137

138 139

140

141

142

143

144 145

146

147

148

149

150

151 152

153

154 155

156

157

158 159

160 161

162

163

164

For the EEG/EMG exploration and sleep experiments, mice underwent a second surgery at least one week after implantation of the telemetry device. Mice were anaesthetized with isoflurane and injected s.c. with meloxicam (2 mg/kg of body weight) for analgesia. After positioning in a stereotaxic frame (Kopf Instruments), mice were implanted with four miniature screw electrodes (from bregma: AP +1.5 and ML +1.5 (ground); AP +1.5 and ML -1.5 (common reference); AP -1.5 and ML -1.5 (EEG 1); AP -1.5 and ML +1.5 (EEG 2) and two EMG electrodes (inserted into neck musculature). These electrodes were each connected, via an insulated wire, to a different gold pin of a EEG/EMG headstage. The EEG/EMG headstage was affixed to the skull using dental adhesive resin cement (Super-Bond C&B). Mice were allowed to recover for a further week before participating in head-fixed and then freely moving behaviour experiments.

Data acquisition of the telemetric thoracic pressure signal

A commercial telemetry system associated with the probes (TSE systems) was used for the wireless recording of the thoracic pressure signals in awake animals. The signal from the probe's transmitter was sensed by the antenna of the telemetry system output which was connected to DAQ (CED Micro1401 with ADC12 expansion, Cambridge Electronic Design Limited, UK) and controlled by spike2 (Cambridge Electronic Design Limited, UK) on a computer. The signal was sampled at 1 KHz by the sensor and digitized at 10 KHz for the experiments on head-fixed animals (to synchronise with the flow sensor recording) and downsampled to 400 Hz for the experiments involving freely-moving animals (to synchronise with the EEG/EMG recording).

Because the implanted probe has a fixed battery life, we could not acquire the thoracic pressure signal continuously. We therefore acquired in 0.5 – 2 minute bursts, with onset timed according to each experiment (before object introduction in the exploration experiment, and after online detection of NREM sleep in the sleep experiments).

175 176

177

178 179

165

166 167

168

169

170

171

172

173 174

Data acquisition of the nasal flow sensor signal

A mass flow sensor (FBAM200DU, SensorTechnics) was used to measure the flow change in front of the nostril thus generating a continuous respiration signal as described previously (34). The signal was digitized at 10 KHz simultaneously with the thoracic pressure signal using the same CED Micro1401 DAQ.

180 181

182

183

184

185 186

187

188 189

190

Head-fixed experiments

The animals were placed in a custom-made head-fixation apparatus attached to a treadmill. The flow sensor was placed in front of the nostrils. Following a brief period of habituation (~ 15 minutes), signals from the flow sensor and the thoracic sensor were recorded simultaneously, with acquisition as described above.

Data acquisition of the EEG/EMG signals

EEG and EMG signals were recorded using the Pinnacle 3-channel tethered system (8200-K1-SL; Pinnacle Technology Inc). Signals were filtered by the preamplifier (high pass above 0.5 Hz for EEG and above 10 Hz for EMG) and then recorded at a sample rate of 400 Hz in Spike2, via the same CED Micro1401 DAQ.

191 192

193

194 195

196

197

198

Behavioural experiments

During the behavioural sessions, mice were placed on the floor of a circular open-topped enclosure (50 cm in diameter) and video was recorded using a Raspberry Pi camera mounted on the ceiling (approximately 1.5 m above the enclosure). The camera sent out TTL pulses on a frame-by-frame basis (25 Hz) to the DAQ, which synchronized the respiration recording with the video recording.

200

201

202

203

204

205

206

207 208

209

210 211

212

213

214

215

216

217

218 219

220

221

222 223

224

225

226 227

228

229

230

231

232

- Formal animal tracking of head, centre and tail coordinates was performed offline using Ethovision XT software (Noldus). This allowed us to define exploratory approach and retraction times, and instantaneous velocity for all the frames of each trial. Four types of behavioural experiment were performed, while video, respiration signal and EEG/EMG (in a subset of mice) were recorded:
 - 1. Open arena exploration: The mouse was gently placed in the arena and allowed to explore freely for approximately five minutes.
 - 2. Novel object: Multiple objects (rubber duck, water bottle, nail varnish bottle, empty food hopper, black bottle, muffin toy) were placed in the arena one at a time, far away from the mouse, who was then allowed to approach and explore the object freely for approximately five minutes. Each object was only presented once to each mouse.
 - 3. Novel odour: A glass petri dish containing a tissue piece impregnated with 2 ml of pure odour (ethyl butyrate, 2-hexanone, isopentyl acetate or eucalyptol) was placed in the arena, far away from the mouse. The mouse was then allowed to approach and explore the petri dish freely for approximately five minutes. Each odour was only presented once to each mouse during awake behaviour (but for a second time during sleep, see below).
 - 4. Inaccessible food: A food pellet was placed in a meshed container, which was then placed in the arena, far away from the mouse. The mouse was then allowed to approach and explore the container freely for approximately five minutes. As these food pellets and their smell were already familiar to the mice, these stimuli were presented in 3-4 trials for each mouse.

Sleep experiments

EEG/EMG and respiration signals were recorded as the animal rested in its home cage, during the first half of the light phase. EEG signals were monitored online, to assess the arousal state of the animal in real time. When the animal entered NREM sleep, we waited for approximately ten seconds before turning on the telemetry respiration sensor for one minute. If the animal was still in NREM approximately ten seconds after that, we carefully placed a petri dish containing a tissue piece impregnated with 2 ml of pure odour (ethyl butyrate, 2-hexanone, isopentyl acetate or eucalyptol; as in the awake behaviour experiments, meaning that this was the second presentation of each odour), into the cage (as we did not see any consistent difference between odours, data was pooled across all four odours). Trials where the placement itself woke the animal up were excluded from analysis. The petri dish was left in position in the cage until sniff monitoring for that trial ended (one minute). Trials were separated by at least five minutes.

237 238

239

240

241

242

243

244

245

246

247

248

249

250

251

252

253

254

255

256 257

258

236

233

234 235

Data analysis - Respiratory signals

The data was analysed using custom scripts written in MATLAB R2019 (Mathworks).

Frequency estimate: The raw data was standardized and detrended. Next, one second of data were passed through an autocorrelation routine. The corresponding time of the first peak was estimated and its reciprocal was used to estimate the dominant frequency for that 1s period. This was repeated using a rolling window of one second with a shift of 50 ms between adjacent windows.

For the freely moving experiment with novel cues, we noted the frames of start and end of each exploration bout and included three seconds preceding and following each exploration bout to make up an individual trial. We followed the same method for estimating frequency for all the trials thus extracted. Events with baseline time less than three seconds were discarded. All trials were aligned to the start of exploration. We calculated the average baseline frequency from the first 500 ms of the trial (this typically included ~5 respiration cycles) and the average exploration frequency from the first one second of object exploration (Fig. 5M-O). We then subtracted the baseline frequency from the entire trial to plot change in frequency, and this was averaged over trials and across mice (Fig. 5J-L).

Frequency error calculation (Head-fixed): The frequency estimation for a 1s period was estimated from both the flow sensor data and the thoracic sensor data. Next, the relative error for that 1s was calculated as;

$$Relative\; error = \frac{Freq^{thoracic} - \; Freq^{flow}}{Freq^{flow}}$$

259 260

261

262

263

264

The relative error is then averaged over the entire trial period to get an average relative error for the specific trial. The mean and standard deviation is estimated from all the trials from all the animals.

Inhalation peak detection: The peak of inhalation was detected as the trough of every sniff cycle in the flow sensor signal and the simultaneously recorded

thoracic sensor signal. The peaks were detected using custom written scripts in MATLAB R2019 (Mathworks). The peak detection was manually scrutinized for discrepancies. To compare peak times between the thoracic and the flow sensor; inhalation peaks were detected in the signals recorded from both the sensors. Next, we calculated the difference in time between the 2 near simultaneous occurring peaks. Since the pressure change in the thoracic cavity happens slightly after any flow through the nostrils, it was assumed that the inhalation peak estimated from the flow sensor signal will precede that estimated from the thoracic sensor signal.

Data analysis - Behaviour

Nose, centre, and tail tracking were performed using Ethovision software. We estimated mouse position, head direction, and instantaneous velocity for each video frame of each trial. Mice were considered to have initiated an exploration bout as soon as their nose entered a 2 cm perimeter around the object/odour/food. Retraction time was defined as the next frame in which the mouse's nose moved out of this perimeter space. In general, these definitions were not ambiguous, and classifying exploratory initiation and retraction times either automatically (using Ethovision) or manually (by scrolling frame-by-frame through the video) gave almost identical results.

Data analysis - Vigilance state classification

Arousal states – NREM, REM and wake – were automatically classified using sleep analysis software in Spike2, and then manually verified in 5 second epochs (as in 45). Wakefulness was defined as de-synchronised, low amplitude EEG and tonic EMG with bursts of movement. NREM sleep was defined as synchronised, high amplitude EEG in the delta frequency range (1-4 Hz) and reduced EMG activity relative to wakefulness. REM sleep was defined when EEG had reduced delta power but prominent power in the theta range (4-10 Hz), and EMG showed an absence of muscle tone.

Data analysis – Association between EEG, EMG and novel Respiration (Resp)

297 signals

Pre-processing: Data recorded from the 4 physiology channels (EEG1, EEG2, EMG and Resp) during each experiment were pre-processed before analysis. Exploration behaviour markers derived from video recording were then aligned with the timeline of the physiology recordings, using TTL time frame alignments. To save battery, the respiratory sensor was not activated throughout the whole experiment, and its recording was interrupted during some experiments. Thus, we removed all data points which had no Resp recording and applied a Butterworth filter, with bandpass 0.5-120 Hz. The resulting dataset was then analysed in four frequency bands of interest: Delta (0.5-4 Hz), Theta (4-8 Hz), Alpha (8-12 Hz) and Beta (12-30 Hz). This was achieved using band-specific band-pass filters.

Partial Coherence Estimates: For the exploration experiments, we applied the slowly evolving locally stationary process (SEv-LSP) framework from Fiecas & Ombao (2016) to the pre-processed data. The four channels [EEG1, EEG2, EMG, Resp] recorded during each experiment were treated as a non-stationary 4-dimensional time series. The 4-dimensional time series were cut into small epochs (0.5-2 sec long) which were treated as "locally stationary". The choice of epoch length was chosen differently for each frequency band, to ensure that a single bin always contained approximately five full cycles: Delta band: 2.22 sec; Theta band: 0.83 sec; Alpha band: 0.5 sec; Beta band: = 0.25 sec.

For each experiment, and for each time epoch, the spectral power matrix was estimated using Thomson's multitaper estimate (46) with K=p x 1.5 = 6 sine tapers. After regularisation (47), the spectral matrix estimates were used to derive partial coherences. The partial coherence is a non-parametric measure of conditional independence between pairs of time series, and was used here to assess the relationship between the [EEG1, EEG2, Resp] channels inside each epoch. With p=4 channels, we have Npcoh=6 relationships between pairs of channels. Partial coherence estimates and p-values (H0: partial coherence =0) were derived for all pairs of channels, at each epoch. Results were adjusted for false discovery rate (FDR) across number of pairs and number of epochs in the experiment. This analysis framework produces a set of slowly evolving partial coherences between the [EEG1, EEG2, EMG, Resp] channels, for each experiment and each frequency band of interest, and produces a set of epoch-sized partial coherences for each pair of channels. However we only report partial coherence results for [EEG1, EEG2, Resp], which have been effectively adjusted for EMG effect

Evolving partial coherence during exploration: We then investigated the association between exploration bouts and evolutionary partial coherences between channels derived from the analysis framework described above. We pooled all experiments together and regressed partial coherence estimates against lagged exploration bouts (+/- 3 time bins around exploration bouts), using multiple-multivariate regression in R (version 3.6.1). This was done first on all types of exploration cues (novel objects, odour, food), then split by exploration cue type. The results of interest from the regression models are the estimated change from baseline in partial coherence values before/during/after exploration bouts, with the null hypothesis being that partial coherence values do not change around exploration bouts. This process was performed separately for each frequency band of interest.

Evolving partial coherence during sleep: To investigate the evolutionary partial coherences between channels at the time of odour introduction during sleep, we applied the same strategy as for exploration, but now taking odour introduction as time 0, and evaluating +/- 3 time bins around this point. This was done across all odour types, but only for trials in which the animal remained in NREM sleep for at least 20 seconds after odour introduction. Using multiple-multivariate regression in R (version 4.3.2), we analysed the data using two sets of multiple linear mixed-effect models.

Weighted connectivity graphs: To obtain a baseline picture of direct associations between channels when the mouse was not exploring, we created weighted connectivity graphs. The non-stationary framework was applied as above to open arena trials, with no stimulus present. Only the data points associated with time-periods when the animal was not moving in the open arena (defined as "still", using methods described below in Movement Classification) were retained. These points were then aggregated together, to produce a graphical model (Fig. 6C & Supp. Fig. 6.1A,B), partial coherence estimate between each channel. A line was drawn between any 2 channels if both (a) partial correlation > 0.15 and (b) p-value for partial correlation being greater than 0 was < 0.05. The thickness of each line represents the partial coherence estimate, and solid / dashed lines represent significant / not significant p values, respectively. This analysis was applied separately for the delta, theta, and alpha frequency bands.

Movement Classification: Movement in the open arena trials for each animal was detected using root mean squared (RMS) on EMG, across sliding time bins of 2

secs (irrespective of frequency band of interest), when the absolute RMS exceeded a conservative animal-specific threshold (10-20% of absolute RMS, meaning that muscle activity had to be very low for the animal to be classed as still). The resulting movement detection estimates, which took values of either 0 or 1 for each time point, were cross-validated against video recordings.

Assessment of effect of movement on respiration measurements: To estimate the effect of movement on respiration recordings, we applied a linear mixed effect regression model, where EMG root mean squared is treated as a fixed effect, and is effect individual animal treated as а random (Sniff rate ~EMG root mean squared + (1|Animal ID)). This effectively assesses the correlation between Resp rate and EMG RMS after adjusting for individual animal variation. The resulting correlation coefficient between Resp rate and EMG RMS is calculated from the effect size resulting from the regression model adjusted for standard deviations of Resp rate and EMG RMS. The resulting p-value associated with this correlation coefficient is taken from the regression model. This regression analysis was repeated three times: (1) on all time points, (2) on time points associated with non-moving moments (EMG RMS below animal-specific threshold), and (3) on time points associated with moving moments (EMG RMS above animalspecific threshold),

Spectral power plots: The pre-processed data were used for estimating the band power without regularisation. Band power in the open arena experiment (including moving and non-moving periods, n=3 mice) was extracted from the spectral estimate matrix for each channel (i.e. diagonal entries of the spectral matrix) at each frequency over the range 0.5-20 Hz, and normalised against total average power over the same frequency range.

391 392

366

367 368

369

370

371

372

373 374

375

376

377

378

379 380

381 382

383

384

385 386

387

388

RESULTS

Implanting thoracic pressure sensor in the right jugular vein of mice

To measure respiration in freely moving mice, we implanted 6-8 week old mice with a wireless pressure sensor (Fig. 1A-F). Briefly, after exposing the right jugular vein, we ligated the superior portion of it to stop any blood flow (Fig. 1C). Next, we made a small incision (Fig. 1D) through which we inserted the pressure sensor towards the thoracic cavity while monitoring the pressure signal online (Fig. 1E). Once we reached the optimal position of the probe, the sensor was held in place with an additional ligature around the vein (Fig. 1F). (Figure 1; described in detail in the Materials and Methods section).

Comparing thoracic pressure sensor and flow sensor signals

After recovering from the surgical implantation (> 7 days after surgery), mice were transferred onto a treadmill. After a short habituation session on the treadmill, we recorded the change in thoracic pressure signal using the implanted pressure sensor, and the change in nasal flow using a flow sensor placed in front of the nostrils (Fig. 2A). Both the sensors reflect respiration in the animals. Qualitatively, the signals looked similar, with downward deflection representing inhalation in both recording methods (Fig. 2B, Supp Fig. 2.1). To quantitatively compare these methods, we measured the frequency and peak inhalation time in both signals recorded simultaneously (Fig. 3). Using autocorrelation to estimate the average frequency, we did not observe any significant difference in the estimated frequency (R = 0.914; Linear regression) between the two signals (Fig. 3A-C) and the relative error between respiration frequency measurements derived from thoracic pressure and flow sensor measurements was 0.016±0.009 (mean±SD; n=21 traces; 4 mice, Fig. 3D).

As nasal flow and thoracic pressure reflect different aspects of respiration, there is likely to be a consistent shift in the time at which each signal peaks and knowing this shift could enable "translation" between these signals. We observed that the end of inhalation corresponds to the point of minimum thoracic pressure, and that the peak of inhalation preceded this point by 0.06 ± 0.03 sec (n=350 sniffs; 4 mice). Overall, therefore, we have found that the thoracic pressure signal can be reliably used to measure respiration and to detect the time of peak flow inhalation. While we assume that this linear relationship holds for the higher frequencies

observed during active exploration (below), it is an important caveat that we could only experimentally describe this relationship for the frequencies naturally demonstrated under head-fixation conditions (~2-8 Hz). Interestingly, Reisert et al. (37) were able to describe a similar relationship between thoracic pressure and intranasal pressure across a wider range of sniffing freguencies, and found that the variability in the difference between these two pressure signals was smaller at higher frequencies (their Figure 5).

433 434 435

436

437

438

439

440

441

442

443

444

445

446 447

448

449

450 451

452

453

454 455

456

457 458

459

427

428 429

430

431

432

Freely moving mice have a bimodal respiration frequency not associated with running speed

Next, we used this method to measure respiration in freely moving mice while they explored an open arena. The thoracic pressure recording was acquired after a short period (~2-3 mins) of habituation in a novel arena while movements were video-recorded for post analysis (Fig. 4A-B). The population of respiration recordings from all animals revealed a bimodal distribution of respiration frequency (Fig. 4C) with a small peak at approximately 3 Hz and a larger peak around 11 Hz. (Note that a bimodal distribution was also observed by Reisert et al., 2014, but in their study it was the lower frequencies that were more common. We suggest that this difference may come from the recording arenas – while the Reisert et al.'s mice were in their home cage, our mice were in a large, novel arena, which may have promoted more exploratory sniffing behaviour in the higher frequency range.) The estimated velocity from simultaneously acquired video recordings also showed a bimodal distribution (Fig. 4D) with peaks at approximately 7 cm/s and 40 cm/s. To understand whether respiration frequency was linked to running speed, we quantified the average velocity associated with 2 prominent frequency bands (1-5 Hz and 9-13 Hz) (Fig. 4E) and the average frequency associated with the 2 prominent bands of velocity (1-10 cm/s and 35-45 cm/s) (Fig. 4F). Surprisingly, we did not observe any significant difference in either of the cases (velocity comparison: p = 0.4691; and frequency comparison: p = 0.2501; both unpaired t-tests), suggesting that respiration rate was largely independent of running velocity (Correlation Co-efficient = -0.0071, Fig. 4G). These results suggest that respiration rate is not simply linked to motor activity, and fits with previous work showing similar differences in respiration rhythm (peaks at 3-5 Hz or 9-11 Hz) during head-fixed running on a treadmill (23). Interestingly, recent work has shown that respiration changes are closely linked to subtler behavioural features during exploration, such as rearing and foraging (40).

461 462

463

464

465

466

467

468

469

470

471

472

473

474

475

476

477

478

479

480

481

482

483

460

Exploration of environmental cues significantly increases respiration frequency

We next asked how respiration frequency changes when mice encounter cues such as novel objects (e.g. rubber duck, plastic toys, empty bottles), monomolecular chemical odourants (ethyl butyrate, 2-Hexanone, eucalyptol and amyl acetate) and food (inaccessible pellet). After habituation to an empty arena, we placed a cue from each class into the arena, one at a time in a random order (Fig. 5A-C). We monitored respiration as the mice voluntarily explored these different cues (Fig. 5D-F). We then calculated the respiration frequency across all exploration bouts (Fig. 5G-I) and quantified the change in respiration frequency from the baseline after aligning the trials to the initial exploration video frame (Fig. 5J-L). For all the 3 classes of cues, we observed that the mice increased their respiration frequency significantly (food odour: p = 0.0103; novel object: p = 2.6e-5; and novel odour: p = 0.0394; paired ttests) at the moment of stimulus investigation, even against the relatively high baseline frequency that mice displayed in this exploratory state (Fig. 5M-O). Sniffing rates are well known to increase during tasks which rely on olfactory discrimination (4,6,7,31,48–50), but the present results, along with other results showing increased sniffing during exploratory locomotion even in the absence of any cues (17), suggest that raised respiration may be a general feature of exploration. In turn, neural entrainment to this respiration rhythm may act similarly - but distinctly - to theta oscillations, providing a scaffold for long-range network communication across the brain (23). We therefore sought to examine how the respiration changes during voluntary exploration are related to brain-wide activity in defined frequency bands.

484 485

486

487 488

489 490

491

492

493

Exploration-triggered respiration changes increase or decrease the coupling between respiration and brain activity depending on EEG frequency band

Recent results have shown that cortical dynamics can be altered by changes in respiration, which were triggered experimentally by changes in CO2 levels (19). We sought to test how the sniffing changes during voluntary exploration relate to cortical dynamics.

Using the implanted thoracic pressure sensor in combination with simultaneous EEG/EMG recording (Fig. 6A-B), we first explored how animals'

respiration related to brain activity while the animal was not exploring or engaged in any observable motor activity ("still" in the open arena, classified according to EMG measurement, see Methods). We applied a frequency-domain locally-stationary time series analysis framework (see Methods) under the assumption of stationarity. This allowed us to build a baseline picture of the relation between all four recording channels (2xEEG, 1xEMG, 1xResp). We found that respiration was not significantly related to the EMG channel, but was directly related to the two EEG channels (which were also directly related to each other, and to EMG; Fig. 6C shows this analysis for the theta band, Supp. Fig. 6.1A,B shows the same analysis for delta and alpha bands).

We then used a frequency-domain approach called partial coherence to understand how the links between these channels evolve over a period of exploration. Partial coherence is a non-parametric measure of direct relationships between signals in a multivariate set. It is derived from the spectral density of the entire channel system, at any given frequency. It is valued between 0 and 1, and can be interpreted as the fraction of power shared by any 2 channels (in our case, EEG and Resp, power spectra across animals shown in Fig. 6D), while controlling for the influence of other channel (EMG) (47; and see Methods for more details).

For four frequency domains: (1) delta band, 0-4 Hz; (2) theta band, 4-8 Hz; (3) alpha band, 8-12 Hz; (4) beta band, 12-30 Hz, we examined how the association between EEG and Resp channels changed before, during and after the mice explored environmental cues (whilst controlling for the influence of muscle activity recorded in the EMG channel), using a slowly-evolving locally-stationary (SeLV) framework. We found that, for the delta and theta frequency bands, the partial coherence across channels decreased relative to baseline before and during an exploration bout, increasing again after the animal stopped exploring (Fig. 6E,F). In contrast, for the alpha and beta frequency bands, the partial coherence across channels increased relative to baseline before and during exploration, decreasing again after the animal stopped exploring (significantly so for alpha but not beta; Fig. 6G,H). This suggests that there is a direct relationship between respiration and brain activity, not mediated by muscle movement, which fluctuates significantly during exploration bouts. This change in direct signalling between brain and respiration differed based on frequency band: The relationship between respiration and brain activity in the delta and theta range decreased before and during exploration, while for the higher frequency bands - alpha and beta - the relationship between brain activity and respiration increased before and during exploration. For all frequency bands, these trends were independent of cue class (novel object / chemical odourant / inaccessible food).

Interestingly, Martin et al. (51) found increased coherence in the beta range between the olfactory bulb and hippocampus during an olfactory learning task, and Zhong et al. (17) found that exploration was associated with increased alignment between respiration rhythm and fast gamma oscillations within the olfactory bulb and the prelimbic cortex. Our results suggest that behaviour-dependent association between neural oscillations and respiration-driven rhythms could be a widespread pattern across cortical as well as subcortical areas. They also extend the picture across frequency domains, and it is interesting to note that the decreased relationships between respiration and brain activity occur in frequencies normally associated with rest or sleep (delta and theta), whereas increased association between respiration and brain activity are found within frequencies normally associated with arousal, sensory awareness and attention (alpha and beta).

543 544 545

546

547 548

549

550 551

552

553

554

555 556

528

529 530

531

532

533

534

535 536

537

538

539

540

541

542

Respiration patterns vary across vigilance states

We next examined how respiration varied as the animal cycled through periods of wake and different sleep stages in its home cage. Similar to previous work using different methods of respiration recording (e.g. implanted thermocouples, 17; whole-body plethysmograph, 19), we found that respiration patterns were different between different sleep states (Fig. 7A), tending to be high in frequency and amplitude but highly variable during wake; very regular and low in frequency and amplitude during NREM sleep, and slightly irregular in both frequency and amplitude during REM sleep. Switches between these different respiration signatures occurred almost instantaneously upon transition between different vigilance states (Fig. 7B). The distribution of inter-sniff intervals was different between sleep states, leading to a mean respiration frequency that was highest in wake (mean frequency = 6.79 Hz) and lowest in REM sleep (mean frequency = 3.09 Hz) (Fig. 7C).

558 559

560

557

Odour-triggered respiration changes during NREM sleep do not induce changes in sleep-associated brain rhythms

562 563

564

565

566

567

568

569

570

571

572

573

574

575

576

577

578

579

580

581

582

583

584

585 586

Girin et al. (19) found that the respiration changes induced by alterations in CO2-enriched air were capable of driving brain activity changes during wakefulness but not during sleep. We wanted to explore whether stimulus-induced sniff changes might tell a different story during sleep. We allowed the animal to rest in its home cage while monitoring EEG and EMG signals continuously (Fig. 8A). When the animal entered NREM sleep, we turned on the thoracic pressure sensor (it was not on continuously due to battery constraints - see Methods for details), and subsequently presented an odour to the sleeping animal (Fig. 8B). Within the 20 seconds following odour presentation, animals transitioned to wake 25% of the time, to REM sleep 25% of the time, and stayed in NREM sleep 50% of the time (Fig. 8C-D). When no odour was presented, the animal was more likely to stay in NREM sleep, and respiration did not change (Fig. 8D,E paired t-test, p = 0.16). But in the cases where odour presentation did not trigger a transition out of NREM sleep, we were able to monitor the effects on respiration and brain activity. In such cases, respiration increased (Fig. 8F paired t-test, p = 0.021; cf no change 20 seconds later: Fig. 8G paired t-test, p = 0.79), but no significant change was observed in sleeprelated EEG rhythms (Fig. 8H delta: p = 0.40; theta: p = 0.31; theta:delta ratio: p = 0.91 (not-depicted); paired t-tests). In line with these results (and in opposition to the awake exploration results), we found that directly examining the partial correlation between respiration and brain activity during sleep (exactly as applied during awake exploration, Figure 6E-H), did not reveal a change in coherence at the time of odour introduction (Figure 8I-J). Thus, our sleep results align with Girin et al.'s findings: neither CO2-induced nor stimulus-induced sniff changes appear to drive brain activity changes during sleep.

DISCUSSION

587

588 589

590

591

592

593

594

595 596

597

598

599

600

601

602

603

604

605

606

607

608

609

610

611

612

613

614 615

616

617 618

619

620

We present a new implantation technique for a wireless thoracic pressure sensor, used to monitor respiration in conjunction with brain recording in freely moving mice. After calibrating with head-fixed respiration measurements using flow sensors, we were able to use this method to investigate respiration and its relationship to EEG brain activity in a variety of behavioural contexts: free exploration of novel environments and cues, and across different sleep-wake states.

While changes in respiration in response to olfactory discrimination odour cues have been well documented (4,31,48-50), our data reveal comparable sniffing increases across voluntary exploration episodes of novel odours, novel objects, and inaccessible food. It is worth noting here that the "odour" stimuli are not the only stimuli which have an olfactory component. Food pellets of course have an olfactory component that is both familiar and holds intrinsic value, while the novel objects are each likely to have different odours which may vary in their strength and complexity depending on the type of material. We expect that the mice are using a multimodal (primarily olfactory and visual) approach to explore each class of stimuli, and while the specific neural response within olfactory and visual regions is likely to depend on the relative salience of each cue, our respiration data align with long-standing observations that diverse sensory stimuli (including non-olfactory stimuli) can arouse sniffing (9), suggesting that raised respiration is a general behavioural feature of active exploration in mice. However, there may be subtler links between respiration and behaviour that we have not been able to draw out from the current data. For instance, Liao & Kleinfeld (40) recently showed that the relative phase between head movement and breathing is different depending on whether an exploring animal is rearing or foraging. It would be interesting to repeat our exploration experiment with the addition of head and torso sensors or higher frame-rate videos from multiple angles in combination with unsupervised machine learning analysis (52; 53), to examine whether there are also differences in the respiration-head movement relationship according to whether the animal is exploring objects, odours or food. Such data could help reveal whether this relationship varies continuously across behavioural states, or whether there is something special about respiration during the specific state of foraging, or in cases of novelty versus familiarity.

Given the increasing view that respiration may provide the scaffold for a brainwide rhythm that can help coordinate neural information transfer across brain regions

622 623

624

625

626

627

628

629

630

631

632

633

634

635

636

637

638

639

640

641

642

643

644

645

646

647

648 649

650

651

652

653

654

(13–16,20), we sought to understand how exploratory sniffing in a voluntary, freely moving task was related to cortical activity in specific frequency bands. Using cortical EEG recording we found that, during stimulus approach, there was a decrease in the association between sniffing and EEG activity in both the delta and theta frequency bands. Cortical delta frequency is most prominent during deep sleep, while cortical theta frequency is associated with REM sleep (reviewed in 54), and so it is perhaps intuitive that the respiratory link with these rhythms would be reduced as the mouse makes an active exploratory approach. The partial coherence between respiration and EEG in the alpha band, on the other hand, increases during exploration. Cortical alpha rhythms have long been associated with conscious perception (reviewed in 55), and in particular, the likelihood of awareness has been found to vary with the phase of the alpha rhythm in humans (56; 57,58; 59,60). It may therefore be of great functional benefit to align sniffing with this rhythm when an animal actively examines a new object. We observed a slight (but not significant) increase in the partial coherence between respiration and brain activity in the beta band, which is associated with motor preparation, sensorimotor integration and top-down signalling (comprehensively reviewed in 55). In general, our data show that active exploration of sensory stimuli in a voluntary, freely moving setting trigger sniff changes that show transiently increased association with brain activity in specific frequency bands.

Several recent studies have revealed that neuronal entrainment of different brain rhythms to the respiration rhythm is affected by arousal (17–19,21,22), so we next looked at respiration across different sleep and wake states. We found that sniff amplitude, frequency and variability are different between wakefulness, NREM sleep and REM sleep, and that transitions between these vigilance states trigger instantaneous changes in sniff pattern. These results show that changes in brain state are linked to observable changes in respiratory behaviour, even in the absence of any change in the olfactory environment, and are in line with what has previously been reported in human sleep (61,62).

Interestingly, odour introduction during deep sleep is less likely than other sensory stimuli to produce EEG signs of arousal in humans (63), and may even deepen sleep (64), although these studies did not examine respiratory changes. Here, we found that introducing an odour to the animal's home cage during NREM sleep could trigger an increase in sniffing in the absence of any vigilance state changes, and without significantly altering the partial coherence between respiration

and the dominant sleep brain rhythms. This suggests that, during sleep, active sampling can be modulated even without any obvious changes to the overall arousal state of the brain, and that the association between respiration and brain activity is not as easily altered as during wake. Our results also expand on those of Girin et al. (19), who showed that breathing changes triggered not by an olfactory stimulus but by changes in CO2 concentration, were least capable of driving respiration-related brain activity changes during deep sleep.

Interestingly, in humans it has been found that presentation of a task-associated odour during sleep can improve learning, both in laboratory (65) and real-world (66,67) settings. This cognitive improvement is thought to be the result of Targeted Memory Reactivation (TMR), whereby the content and frequency of hippocampal replay events during sleep are biased by a sensory stimulus (shown with auditory stimuli: 68). Because such replay events would not be detected by the EEG measurements made here, it is possible that the odour presentation during sleep is causing a change to brain activity that we are missing. An additional factor is the salience of the sensory cue presented during sleep - our odours were neither novel (having been presented once during wake) nor associated with any particular task or outcome. It would be interesting to repeat this experiment with task-associated odours and sleep-novel odours, to see whether stimulus salience affects the sniffing response, the EEG response or their coherence in a particular frequency band.

We would like to point out some limitations of the present work. One major drawback of this wireless technique to measure respiration, is that the current version of the implanted device for mice cannot be recharged, so the absolute data collection period is limited to approximately 24 hours. For this reason, the experimenter must make a choice between monitoring in long stretches over 1-2 days or in short bursts over several days / conditions. We chose the latter approach, with each respiration recording lasting between 30 sec to two minutes. This ensured that we were able to do many recordings across different exploratory and vigilance conditions, but of course a different approach would need to be adopted to examine behaviours that evolve over a slower timescale, in which case the number of experimental conditions that an individual mouse could participate in would be smaller. However, this constraint would be less harsh for the rat device, which can house a bigger battery, and may be further reduced in both species with the rise of

690 691

692

693

694

695

696

697

698

699

700

701

702

703

704

705

706

707

708

709

710

711712

713

714

715

716

717

718

719

720

721

722

wireless charging. Improved batteries / charging might also provide the possibility of implanting smaller thoracic pressure sensors in younger animals to allow for developmental studies.

Another potential issue with any new recording technique, is the possibility for signal contamination by unexpected confounds. The confound that we were most concerned with here was movement: if the pressure sensor was affected by locomotion or head movements, for instance, then we could not be sure whether changes in the signal were the result of changes in breathing or in movement. Similarly, we could not meaningfully compare across conditions which differ in movement levels, as is the case for wake and sleep. We therefore carried out multiple tests to examine whether muscle movement was contaminating the respiration signal picked up by the pressure sensor. First, we found that respiration measurements were not correlated with either the speed of mouse locomotion (as measured by video-tracking, Fig. 4E-G), or tone of the neck muscle (as measured by EMG, Supp. Fig. 6.1E). Second, we found that estimates for evolving partial coherence between EEG and respiration did not differ when the mouse was still versus moving (as defined by EMG, Supp. Fig. 6.1C,D). And finally, we examined the weights of the direct associations calculated using stationary coherence, and found that the link between respiration and EMG was the smallest across frequency bands (Fig 6C; Supp. Fig. 6.1A,B). We are therefore relatively confident in this case that movement artefacts did not impact the respiration measurements made by the implanted pressure sensor. We cannot rule out that the sensor might pick-up movement to some degree, but if this were the case here, the respiration signal was certainly strong enough not to be affected by it.

In summary, we have used a new surgical technique to implant a telemetry-based thoracic pressure sensor, and have shown that this can be used to accurately measure respiration in freely moving mice. Since respiration rhythm is increasingly being viewed as an important brain-wide scaffold to which other neural rhythms can align, we combined this new measurement technique with implanted EEG and EMG to monitor brain activity in specific frequency bands during behaviour and across vigilance states. During stimulus exploration, the association between respiration and cortical delta and theta decreased, but the association between respiration with alpha increased. Odour presentation during sleep was able to cause a transient increase in sniffing, but did not appear to change dominant sleep rhythms in the

cortex. Overall, our data align with the idea that respiration may be a useful driver for synchronising specific brain rhythms, particularly during wakefulness and exploration, but during sleep, respiratory changes seem less able to impact EEG measures of brain activity.

Having demonstrated the flexibility with which thoracic pressure sensing can be combined with different behavioural assays and brain recording, we anticipate that this wireless technique to measure respiration will provide many new insights into the way that animals use olfactory information to understand the environment. Our recent findings show that mice can compute sub-sniff level information (32,34), and it will next be important to interrogate how the relationship between respiration and specific brain rhythms contributes to sub-sniff level computation in freely moving animals.

735

723

724 725

726

727

728

729

730

731

732

733

ACKNOWLEDGEMENTS

This work was supported by the Francis Crick Institute which receives its core funding from Cancer Research UK (CC2036), the UK Medical Research Council (CC2036), and the Wellcome Trust (CC2036); by the UK Medical Research Council (grant reference MC_UP_1202/5); a Wellcome Trust Investigator grant to ATS (110174/Z/15/Z) and the National Science Foundation/Canadian Institute of Health Research/German Research Foundation/Fonds de Recherche du Québec/UK Research and Innovation–Medical Research Council Next Generation Networks for Neuroscience Program (Award No. 2014217). We thank Yolanda Saavedra Torres and Rene Remie for helping in the standardisation process of the surgical procedure. We thank the animal facilities at National Institute for Medical Research and the Francis Crick Institute for animal care and technical assistance. We thank Matthew Wachowiak, Johannes Reisert and Mihaly Kollo for their helpful comments on earlier versions of the manuscript. For the purpose of Open Access, the author has applied a CC BY public copyright licence to any Author Accepted Manuscript version arising from this submission.

ADDITIONAL INFORMATION

Data Availability

The data that support the findings of this study are available from the corresponding author, upon reasonable request.

Competing Interests

760 The authors declare no conflicts of interest.

Supplemental material available at:

- 763 DOI: 10.6084/m9.figshare.25624752
- 764 https://figshare.com/s/724d47b267538145fe96

FIGURE LEGENDS

767

768

766

Figure 1. Jugular vein implantation of thoracic pressure sensor

- 769 (A) Schema showing the final location of the pressure sensor tip in the jugular vein
- and the subcutaneous location of the transmitter on the back (B). (C-F) The critical
- steps of the surgery are tying the rostral knot on the right jugular vein (C); making the
- incision on the jugular vein (D); inserting the sensor tip through the incision towards
- the heart (E) and securing the sensor at the correct position for optimal signal (F).

774

775

Figure 2. Head-Fixed experimental setup for simultaneous measurement from

- 776 nasal flow sensor and thoracic pressure sensor
- 777 (A) A schematic diagram of the experimental setup used for simultaneous
- 778 measurement of real-time respiration signals using a flow sensor placed near the
- nostrils and a thoracic sensor implanted in the jugular vein of head-fixed mice.
- 780 (B) An example recording obtained simultaneously from the flow sensor (red) and
- the thoracic sensor (blue). A zoomed section is shown at the right.

782

783

Figure 3. Implanted thoracic sensor is a reliable way of measuring respiration

- 784 in awake mice
- 785 (A) An example recording obtained simultaneously using a flow sensor (red) and a
- thoracic sensor (blue) in a head-fixed mouse.
- 787 (B) Average frequency (estimated using autocorrelation with a rolling 1 sec window,
- see Methods) from the 2 traces in (A).
- 789 (C) Frequency estimate using the thoracic sensor vs flow sensor. Each marker
- 790 represents the average frequency obtained from 1s segment of a trial. (Linear
- Regression analysis, R = 0.914, P<0.001). Different colours represent different
- 792 animals.
- (D) Error fraction in estimating frequency from the same traces as in (C).

- 794 (E) An example stretch of sniffs demonstrating the consistency of time-interval
- between the measured inhalation peak using the 2 sensors.
- 796 (F) Time-interval between the inhalation peak times measured from the 2 sensors
- simultaneously. The colours represent the same animals as in (C). Solid markers
- 798 represent mean±SD. The black marker represents the population average time-
- 799 interval of -0.06 ± 0.03 s.
- 800 (G) Histogram of the population of time difference in inhalation peak obtained from
- 801 all the sniffs in (F), n=350.

- Figure 4. Respiration measurement from freely moving mice implanted with
- 804 thoracic sensors exploring an open arena
- 805 (A) A schema of the experimental setup used for telemetry recording of respiration in
- 806 freely moving animals in an open arena.
- 807 (B) An example trace of respiration recording from an animal while it freely navigated
- in the open arena (*Top*). Note the respiration profiles in the 2 zoomed sections
- during high frequency respiration, low velocity movement (*left*) and high frequency,
- 810 high velocity (*right*).
- 811 (C) Histogram of respiration frequency estimate from all animals (n=4 animals).
- Brown and green indicate the range of frequencies analysed in (E).
- 813 (D) Histogram of running velocity from all animals in (C). Brown and green indicate
- the range of velocities analysed in (F).
- 815 (E) Average running velocity was independent from respiration frequency in
- frequency ranges between 1-5 Hz (brown) and 9-13 Hz (green, indicated in C).
- (F) Average respiration frequency was independent from running velocity at speeds
- of 1-10 cm/s (brown) and 35-45 cm/s (green, indicated in D).
- 819 (G) Running velocity vs. respiration frequency does not show any substantial
- s20 correlation (R = -0.0071, dotted line) from all the animals in (C).

Figure 5. Mice show increased respiration frequency during exploring novel

- 823 food, object and odour
- (A) A schematic diagram of the experimental setup used for mice exploring food, (B)
- a novel object and (C) a novel odour while recording their respiration.
- 826 (D) An example respiration recording (top) and its corresponding respiration
- frequency estimate (bottom) for a trial where an inaccessible piece of food was
- placed in the arena. The cream bar denotes the time of exploration in that trial (E)
- Similar example for a trial in which a novel object and novel odour (F) were placed in
- the arena.
- (G) Respiration frequency plots from multiple trials performed by an animal exploring
- the inaccessible food, novel object (H) and novel odour (I). Note the change in sniff
- frequency during the exploration time. Dotted line indicates the time at which the
- animal stopped exploring for each trial.
- 835 (J) Baseline subtracted respiration frequency plotted against time for inaccessible
- 836 food (n=85), novel object (n=134) (K) and novel odour (n=72) (L). The thick lines
- represent the mean and the shaded region represents the sem (4 mice).
- 838 (M) Respiration frequency during the period of exploration significantly increases
- 839 from the baseline respiration frequency for inaccessible food (p = 0.0014), novel
- object (p<0.001) (N) and novel odour (p = 0.03) (O) (4 mice).

Figure 6. EEG, EMG and sniff relationships during freely moving awake

843 **behaviour**

- (A) Schematic of EEG/EMG electrode placement (top) and mouse implanted with
- both thoracic sensor and EEG/EMG recording devices (bottom).
- (B) Example raw traces from each of the four recording channels.
- 847 (C) Graphical representation of the baseline relationships between the four recording
- channels. Partial coherence between each channel was estimated while the animals
- 849 were awake but not moving in an open arena, in the absence of additional
- environmental cues. A line was drawn between any 2 channels if both (a) partial
- correlation > 0.15 and (b) p-value for partial correlation being greater than 0 was <

- 0.05. The thickness of each line represents the partial coherence estimate, and solid / dashed lines represent significant / not significant p values, respectively. This plot is for the Theta band (see Supp. Fig. 6.1 for other bands).
- 855 (D) Spectral power plots for EEG and Resp channels recorded in the open arena 856 (including moving and not moving epochs), showing brain activity and breathing 857 signals in the delta-beta frequency ranges (n=3 mice).(E-H) Estimates of changes in 858 partial coherence between channel pairs in time bins before (negative time lag), during (0 time lag) and after (positive time lag) an animal explores an introduced 859 860 environmental cue (either novel object, novel odour or food odour). Analysis was 861 done separately for different frequency bands: delta (D; 4 mice), theta (E; 4 mice), alpha (F; 4 mice), and beta (G; 4 mice). Key for significance: "*" = p<0.01; "= p 862 863 p<0.05; '.' = p<0.1.

865

Figure 7. Respiration frequency changes with vigilance state

- (A) Raw example sniff, EEG and EMG signals in wake (blue), NREM (green) and REM (cyan) sleep. The respiration trace (top row) shows that respiration is varied and often large in amplitude during wake, highly regular and low in amplitude during NREM sleep, and slightly irregular during REM sleep. Respiration frequency tends to
- be high during wake and lower in NREM and REM sleep (zoomed in boxes).
- (B) Changes in respiration are seen almost instantaneously upon transition between
- different vigilance states (note, mammals typically do not transition from REM to
- NREM sleep).
- (C) Distributions of inter-sniff intervals for wake, NREM and REM sleep, with mean respiration frequency for each state given in Hz.

876

877

Figure 8. Odour presentation during sleep

(A) Schematic of recording set up. While the animal was sleeping, EEG/EMG and respiration signals were recorded, and odours were placed in the animal's home cage.

- 881 (B) Schematic of analysis framework. Ten seconds after the animal entered NREM 882 sleep (switch from blue to green, top row), the respiration sensor was turned on (for 883 one minute; grey line, middle row). Ten seconds later, odour was placed into the
- cage and the window for detecting state transitions was opened (for 20 seconds,
- blue shaded square). The red and black shaded squares represent the timing of
- 886 respiration frequency comparisons (panels E-G) and EEG frequency band
- 887 comparisons (H-J).
- 888 (C) Raw example traces of respiration, EEG and EMG signals for an instance when
- the animal transitioned to wake, REM or NREM, within 20 seconds of odour
- 890 presentation.
- (D) Pie charts showing proportion of state transitions that occurred between 20-40s
- from the onset of NREM sleep, for cases where odour was not presented (left pie
- chart) and cases where odour was presented at t=20s (right pie chart). While odour
- presentation did increase the proportion of transitions to wake and REM sleep, in
- half the cases, odour presentation did not cause the mouse to switch out of NREM
- sleep (10 out of 20 trials, across two mice).
- 897 (E) In three trials, the respiration sensor was turned on without any odour being
- presented. In these cases, respiration frequency did not change 20 seconds after the
- start of NREM sleep (left: dark green line represents mean across trials, shaded
- 900 region represents SEM; right: paired t-test, p = 0.16, two shapes represent two
- 901 mice).
- 902 (F) In the cases where odour presentation did not cause transition out of NREM
- 903 sleep, there was a significant increase in the average respiration frequency (paired t-
- test, p = 0.021; colours and shapes as in E).
- 905 (G) Control comparisons made 20 seconds after odour presentation (in cases where
- animal was still in NREM sleep) did not reveal a change in average respiration
- 907 frequency (paired t-test, p = 0.79; colours and shapes as in E).
- 908 (H) In cases where odour presentation did not cause transition out of NREM sleep,
- there was no significant change in the EEG delta power (H; p = 0.40) or theta power
- 910 (I; p = 0.31)(colours as in E-G; p values are from paired t-tests, comparing average
- 911 values for five seconds shown in red vs five seconds shown in black, as in E-G).

(I,J) Estimates of changes in partial coherence between channel pairs in time bins before (negative time lag), during (0 time lag) and after (positive time lag) an odour was introduced to the animal during NREM sleep (as for F-H, only including trials in which the animal remained in NREM sleep, 10 trials across two mice). Analysis was done separately for the dominant sleep frequency bands: delta and theta. Key for significance is the same as in 6E-H.

918

912

913

914 915

916

917

REFERENCES

- 1. Schroeder, C. E., Wilson, D. A., Radman, T., Scharfman, H. & Lakatos, P.
- Dynamics of Active Sensing and perceptual selection. *Current Opinion in*
- 923 Neurobiology **20**, 172–176 (2010).
- 924 2. Margrie, T. W. & Schaefer, A. T. Theta oscillation coupled spike latencies yield
- computational vigour in a mammalian sensory system. *The Journal of Physiology*
- 926 **546**, 363–374 (2003).
- 3. Kepecs, A., Uchida, N. & Mainen, Z. F. The Sniff as a Unit of Olfactory
- 928 Processing. *Chemical Senses* **31**, 167–179 (2006).
- 929 4. Verhagen, J. V., Wesson, D. W., Netoff, T. I., White, J. A. & Wachowiak, M.
- Sniffing controls an adaptive filter of sensory input to the olfactory bulb. *Nat*
- 931 *Neurosci* **10**, 631–639 (2007).
- 5. Cenier, T., McGann, J. P., Tsuno, Y., Verhagen, J. V. & Wachowiak, M. Testing
- the sorption hypothesis in olfaction: a limited role for sniff strength in shaping
- 934 primary odor representations during behavior. *J Neurosci* **33**, 79–92 (2013).
- 935 6. Jordan, R., Fukunaga, I., Kollo, M. & Schaefer, A. T. Active Sampling State
- 936 Dynamically Enhances Olfactory Bulb Odor Representation. Neuron 98, 1214-
- 937 1228.e5 (2018).
- 7. Jordan, R., Kollo, M. & Schaefer, A. T. Sniffing Fast: Paradoxical Effects on Odor
- 939 Concentration Discrimination at the Levels of Olfactory Bulb Output and
- 940 Behavior. *eNeuro* **5**, ENEURO.0148-18.2018 (2018).
- 8. Shusterman, R., Sirotin, Y. B., Smear, M. C., Ahmadian, Y. & Rinberg, D. Sniff
- 942 Invariant Odor Coding. *eNeuro* **5**, ENEURO.0149-18.2018 (2018).
- 943 9. Welker, W. I. Analysis of Sniffing of the Albino Rat 1). *Behav* **22**, 223–244 (1964).

- 944 10. Youngentob, S. L., Mozell, M. M., Sheehe, P. R. & Hornung, D. E. A quantitative
- 945 analysis of sniffing strategies in rats performing odor detection tasks. *Physiology*
- 946 & Behavior **41**, 59–69 (1987).
- 947 11. Wachowiak, M. All in a Sniff: Olfaction as a Model for Active Sensing. *Neuron* 71,
- 948 962–973 (2011).
- 949 12. Folschweiller, S. & Sauer, J.-F. Controlling neuronal assemblies: a fundamental
- 950 function of respiration-related brain oscillations in neuronal networks. Pflugers
- 951 *Arch - Eur J Physiol* **475**, 13–21 (2023).
- 952 13. Kleinfeld, D., Deschênes, M., Wang, F. & Moore, J. D. More than a rhythm of life:
- 953 breathing as a binder of orofacial sensation. Nat Neurosci 17, 647–651 (2014).
- 954 14. Heck, D. H. et al. Breathing as a Fundamental Rhythm of Brain Function. Front.
- 955 Neural Circuits **10**, (2017).
- 956 15. Tort, A. B. L., Brankačk, J. & Draguhn, A. Respiration-Entrained Brain Rhythms
- 957 Are Global but Often Overlooked. *Trends Neurosci* 41, 186–197 (2018).
- 958 16. Heck, D. H., Kozma, R. & Kay, L. M. The rhythm of memory: how breathing
- 959 shapes memory function. Journal of Neurophysiology 122, 563–571 (2019).
- 960 17. Zhong, W. *et al.* Selective entrainment of gamma subbands by different slow
- 961 network oscillations. *Proc. Natl. Acad. Sci. U.S.A.* **114**, 4519–4524 (2017).
- 962 18. Cavelli, M. et al. Nasal respiration entrains neocortical long-range gamma
- 963 coherence during wakefulness. Eur J of Neuroscience 51, 1463–1477 (2020).
- 19. Girin, B. et al. The deep and slow breathing characterizing rest favors brain 964
- 965 respiratory-drive. *Sci Rep* **11**, 7044 (2021).
- 966 Sheriff, A., Pandolfi, G., Nguyen, V. S. & Kay, L. M. Long-Range Respiratory and
- 967 Theta Oscillation Networks Depend on Spatial Sensory Context. J. Neurosci. 41,
- 968 9957–9970 (2021).

- 21. Tort, A. B. L., Hammer, M., Zhang, J., Brankačk, J. & Draguhn, A. Temporal
- 970 Relations between Cortical Network Oscillations and Breathing Frequency during
- 971 REM Sleep. *J. Neurosci.* **41**, 5229–5242 (2021).
- 22. Karalis, N. & Sirota, A. Breathing coordinates cortico-hippocampal dynamics in
- mice during offline states. *Nat Commun* **13**, 467 (2022).
- 23. Nguyen Chi, V. et al. Hippocampal Respiration-Driven Rhythm Distinct from
- Theta Oscillations in Awake Mice. *J. Neurosci.* **36**, 162–177 (2016).
- 24. Grimaud, J. & Murthy, V. N. How to monitor breathing in laboratory rodents: a
- review of the current methods. *Journal of Neurophysiology* **120**, 624–632 (2018).
- 25. Walker, J. K. L., Lawson, B. L. & Jennings, D. B. Breath timing, volume and drive
- to breathe in conscious rats: comparative aspects. Respiration Physiology 107,
- 980 241–250 (1997).
- 26. Lim, R. et al. Measuring Respiratory Function in Mice Using Unrestrained Whole-
- body Plethysmography. *JoVE* 51755 (2014) doi:10.3791/51755.
- 983 27. Matrot, B. *et al.* Automatic classification of activity and apneas using whole body
- 984 plethysmography in newborn mice. *Journal of Applied Physiology* **98**, 365–370
- 985 (2005).
- 986 28. Prada-Dacasa, P., Urpi, A., Sánchez-Benito, L., Bianchi, P. & Quintana, A.
- 987 Measuring Breathing Patterns in Mice Using Whole-body Plethysmography. *Bio*
- 988 *Protoc* **10**, e3741 (2020).
- 989 29. Fukunaga, I., Berning, M., Kollo, M., Schmaltz, A. & Schaefer, A. T. Two Distinct
- 990 Channels of Olfactory Bulb Output. *Neuron* **75**, 320–329 (2012).
- 991 30. Zehendner, C. M., Luhmann, H. J. & Yang, J.-W. A simple and novel method to
- monitor breathing and heart rate in awake and urethane-anesthetized newborn
- 993 rodents. *PLoS One* **8**, e62628 (2013).

- 31. Esquivelzeta Rabell, J., Mutlu, K., Noutel, J., Martin Del Olmo, P. & Haesler, S.
- Spontaneous Rapid Odor Source Localization Behavior Requires
- Interhemispheric Communication. *Current Biology* **27**, 1542-1548.e4 (2017).
- 997 32. Ackels, T. et al. Fast odour dynamics are encoded in the olfactory system and
- guide behaviour. *Nature* **593**, 558–563 (2021).
- 999 33. Bolding, K. A. & Franks, K. M. Complementary codes for odor identity and
- intensity in olfactory cortex. *eLife* **6**, e22630 (2017).
- 1001 34. Dasgupta, D., Warner, T. P. A., Erskine, A. & Schaefer, A. T. Coupling of Mouse
- Olfactory Bulb Projection Neurons to Fluctuating Odor Pulses. J. Neurosci. 42,
- 1003 4278–4296 (2022).
- 35. Oka, Y., Takai, Y. & Touhara, K. Nasal Airflow Rate Affects the Sensitivity and
- Pattern of Glomerular Odorant Responses in the Mouse Olfactory Bulb. *J.*
- 1006 Neurosci. **29**, 12070–12078 (2009).
- 36. Shusterman, R., Smear, M. C., Koulakov, A. A. & Rinberg, D. Precise olfactory
- responses tile the sniff cycle. *Nat Neurosci* **14**, 1039–1044 (2011).
- 1009 37. Reisert, J. et al. Comparing thoracic and intra-nasal pressure transients to
- monitor active odor sampling during odor-guided decision making in the mouse.
- 1011 *Journal of Neuroscience Methods* **221**, 8–14 (2014).
- 38. Sirotin, Y. B., Costa, M. E. & Laplagne, D. A. Rodent ultrasonic vocalizations are
- bound to active sniffing behavior. *Front Behav Neurosci* **8**, 399 (2014).
- 39. Ito, J. et al. Whisker barrel cortex delta oscillations and gamma power in the
- awake mouse are linked to respiration. *Nat Commun* **5**, 3572 (2014).
- 40. Liao, S.-M. & Kleinfeld, D. A change in behavioral state switches the pattern of
- motor output that underlies rhythmic head and orofacial movements. Current
- 1018 Biology **33**, 1951-1966.e6 (2023).

- 41. Liu, S. et al. Divergent brainstem opioidergic pathways that coordinate breathing
- with pain and emotions. *Neuron* **110**, 857-873.e9 (2022).
- 42. Liu, S. & Han, S. Simultaneous recording of breathing and neural activity in
- awake behaving mice. *STAR Protocols* **3**, 101412 (2022).
- 1023 43. Macrides, F. Temporal relationships between hippocampal slow waves and
- exploratory sniffing in hamsters. *Behavioral Biology* **14**, 295–308 (1975).
- 44. McAfee, S. S. *et al.* Minimally invasive highly precise monitoring of respiratory
- rhythm in the mouse using an epithelial temperature probe. *Journal of*
- 1027 Neuroscience Methods **263**, 89–94 (2016).
- 45. Harris, J. J., Kollo, M., Erskine, A., Schaefer, A. & Burdakov, D. Natural VTA
- activity during NREM sleep influences future exploratory behavior. *iScience* **25**,
- 1030 104396 (2022).
- 46. Riedel, K. S. & Sidorenko, A. Minimum bias multiple taper spectral estimation.
- 1032 *IEEE Trans. Signal Process.* **43**, 188–195 (1995).
- 1033 47. Schneider-Luftman, D. & Walden, A. T. Partial Coherence Estimation via
- Spectral Matrix Shrinkage under Quadratic Loss. *IEEE Trans. Signal Process.*
- 1035 **64**, 5767–5777 (2016).
- 48. Coronas-Samano, G., Ivanova, A. V. & Verhagen, J. V. The Habituation/Cross-
- Habituation Test Revisited: Guidance from Sniffing and Video Tracking. *Neural*
- 1038 *Plasticity* **2016**, 1–14 (2016).
- 49. Wesson, D. W., Carey, R. M., Verhagen, J. V. & Wachowiak, M. Rapid Encoding
- and Perception of Novel Odors in the Rat. *PLoS Biol* **6**, e82 (2008).
- 50. Wesson, D. W., Donahou, T. N., Johnson, M. O. & Wachowiak, M. Sniffing
- Behavior of Mice during Performance in Odor-Guided Tasks. Chemical Senses
- **33**, 581–596 (2008).

- 51. Martin, C., Beshel, J. & Kay, L. M. An Olfacto-Hippocampal Network Is
- Dynamically Involved in Odor-Discrimination Learning. *Journal of*
- 1046 *Neurophysiology* **98**, 2196–2205 (2007).
- 52. Wiltschko, A. B. *et al.* Mapping Sub-Second Structure in Mouse Behavior.
- 1048 *Neuron* **88**, 1121–1135 (2015).
- 53. Mathis, A. et al. DeepLabCut: markerless pose estimation of user-defined body
- parts with deep learning. *Nat Neurosci* **21**, 1281–1289 (2018).
- 54. Poe, G. R., Walsh, C. M. & Bjorness, T. E. Cognitive neuroscience of sleep. in
- 1052 Progress in Brain Research vol. 185 1–19 (Elsevier, 2010).
- 55. Wang, X.-J. Neurophysiological and Computational Principles of Cortical
- 1054 Rhythms in Cognition. *Physiological Reviews* **90**, 1195–1268 (2010).
- 56. Ergenoglu, T. *et al.* Alpha rhythm of the EEG modulates visual detection
- performance in humans. *Brain Res Cogn Brain Res* **20**, 376–383 (2004).
- 57. Busch, N. A., Dubois, J. & VanRullen, R. The phase of ongoing EEG oscillations
- predicts visual perception. *J Neurosci* **29**, 7869–7876 (2009).
- 58. van Dijk, H., Schoffelen, J.-M., Oostenveld, R. & Jensen, O. Prestimulus
- oscillatory activity in the alpha band predicts visual discrimination ability. *J*
- 1061 *Neurosci* **28**, 1816–1823 (2008).
- 59. Mathewson, K. E., Gratton, G., Fabiani, M., Beck, D. M. & Ro, T. To see or not to
- see: prestimulus alpha phase predicts visual awareness. *J Neurosci* **29**, 2725–
- 1064 2732 (2009).
- 1065 60. Wyart, V. & Sergent, C. The phase of ongoing EEG oscillations uncovers the fine
- temporal structure of conscious perception. *J Neurosci* **29**, 12839–12841 (2009).
- 61. Gutierrez, G. et al. Respiratory rate variability in sleeping adults without
- obstructive sleep apnea. *Physiol Rep* **4**, e12949 (2016).

1069	62. Reed, C. I. & Kleitman, N. STUDIES ON THE PHYSIOLOGY OF SLEEP: IV. T
1070	HE E FFECT OF S LEEP ON R ESPIRATION. American Journal of Physiology-Legacy
1071	Content 75 , 600–608 (1926).
1072	63. Carskadon, M. A. & Herz, R. S. Minimal olfactory perception during sleep: why
1073	odor alarms will not work for humans. Sleep 27, 402–405 (2004).
1074	64. Perl, O. et al. Odors enhance slow-wave activity in non-rapid eye movement
1075	sleep. Journal of Neurophysiology 115, 2294–2302 (2016).
1076	65. Rasch, B., Büchel, C., Gais, S. & Born, J. Odor Cues During Slow-Wave Sleep
1077	Prompt Declarative Memory Consolidation. Science 315, 1426–1429 (2007).
1078	66. Knötzele, J. et al. Presenting rose odor during learning, sleep and retrieval helps
1079	to improve memory consolidation: a real-life study. Sci Rep 13, 2371 (2023).
1080	67. Vidal, V. et al. Odor cueing during sleep improves consolidation of a history
1081	lesson in a school setting. <i>Sci Rep</i> 12 , 10350 (2022).
1082	68. Bendor, D. & Wilson, M. A. Biasing the content of hippocampal replay during
1083	sleep. Nat Neurosci 15, 1439–1444 (2012).
1084	
1085	

 $Downloaded\ from\ journals.physiology.org/journal/jn\ (2601:08C0:0600:F9EB:2586:016C:C2CD:D04C)\ on\ July\ 15,2024. \quad \textbf{38}$

Fig 1. Thoracic sensor implantation

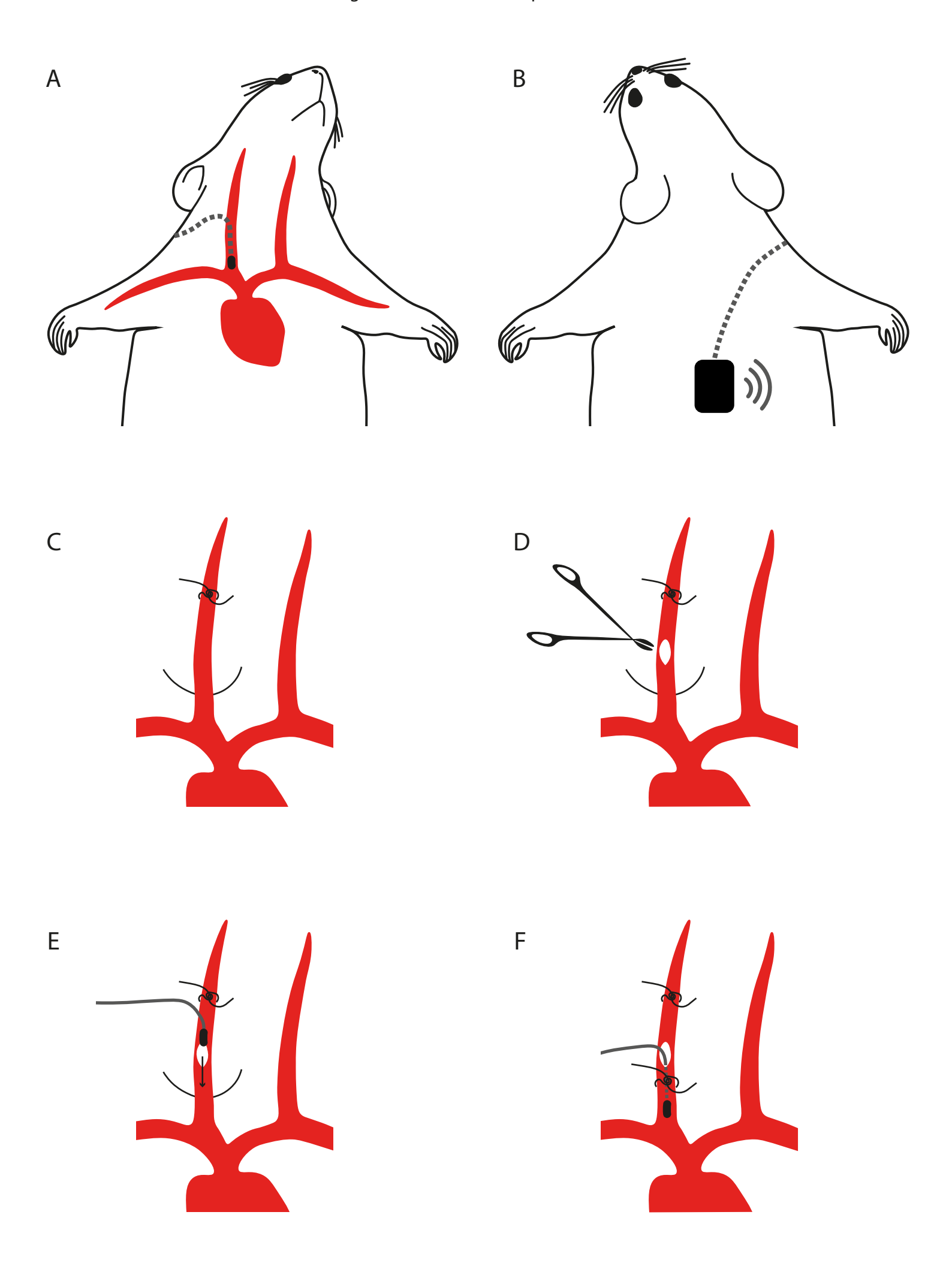
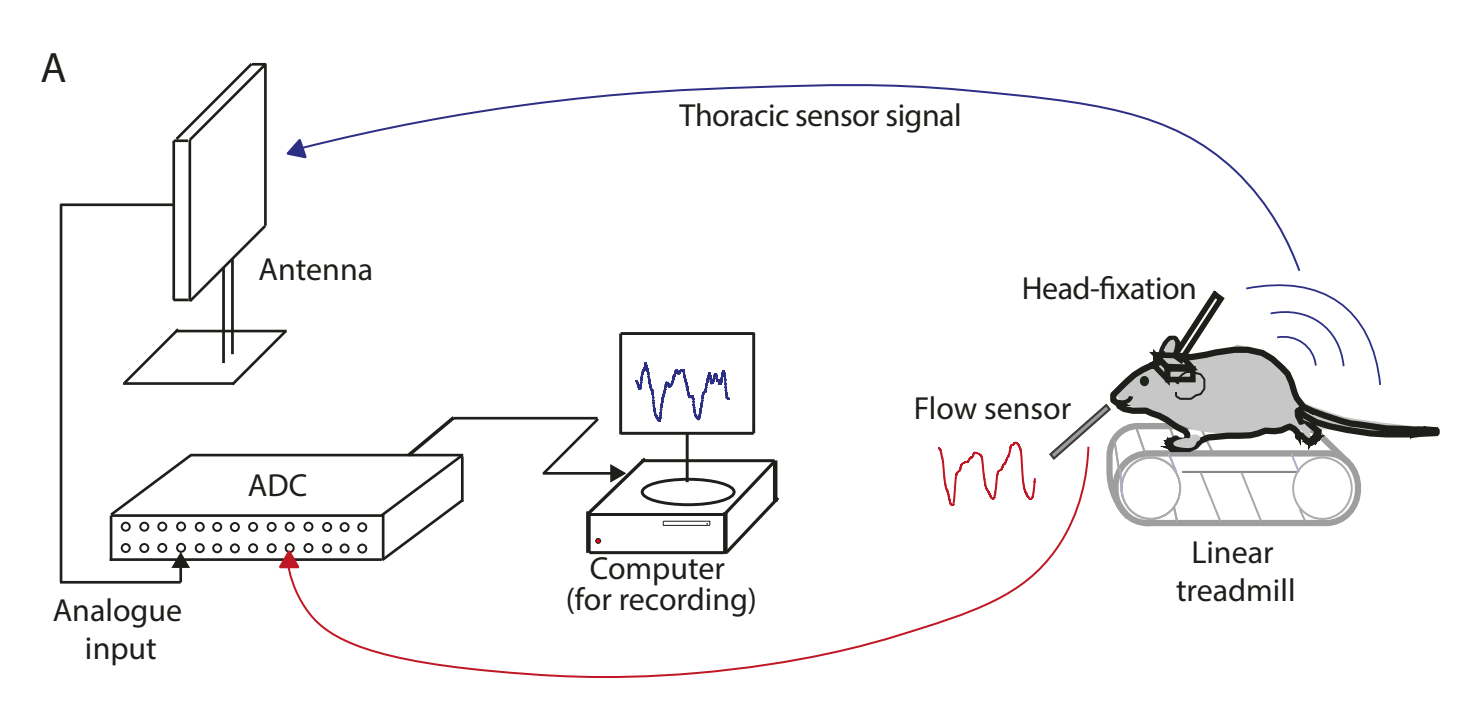


Fig 2. Head-fixed schema and demo trace



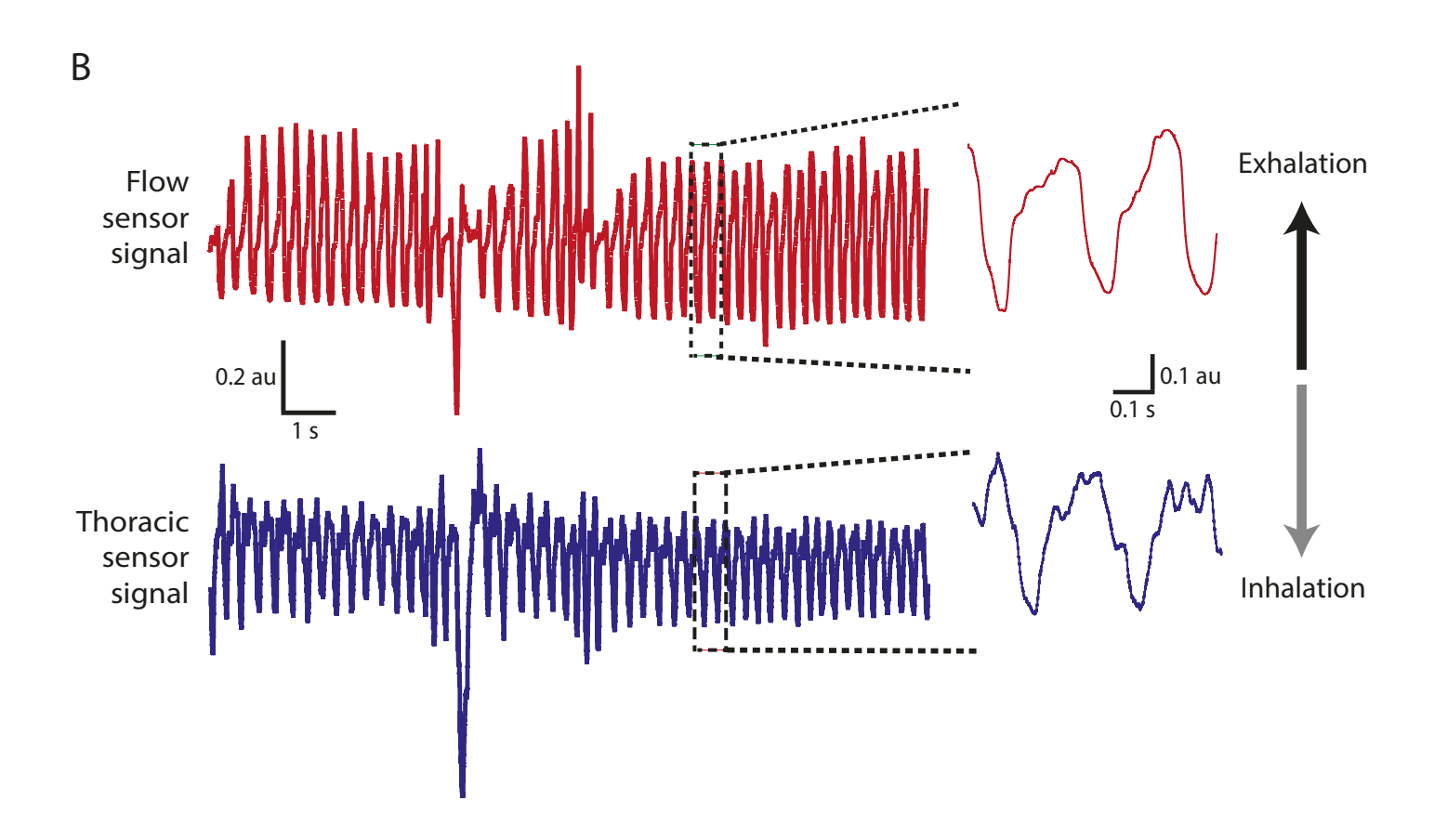


Fig 3. Head-Fixed Analysis

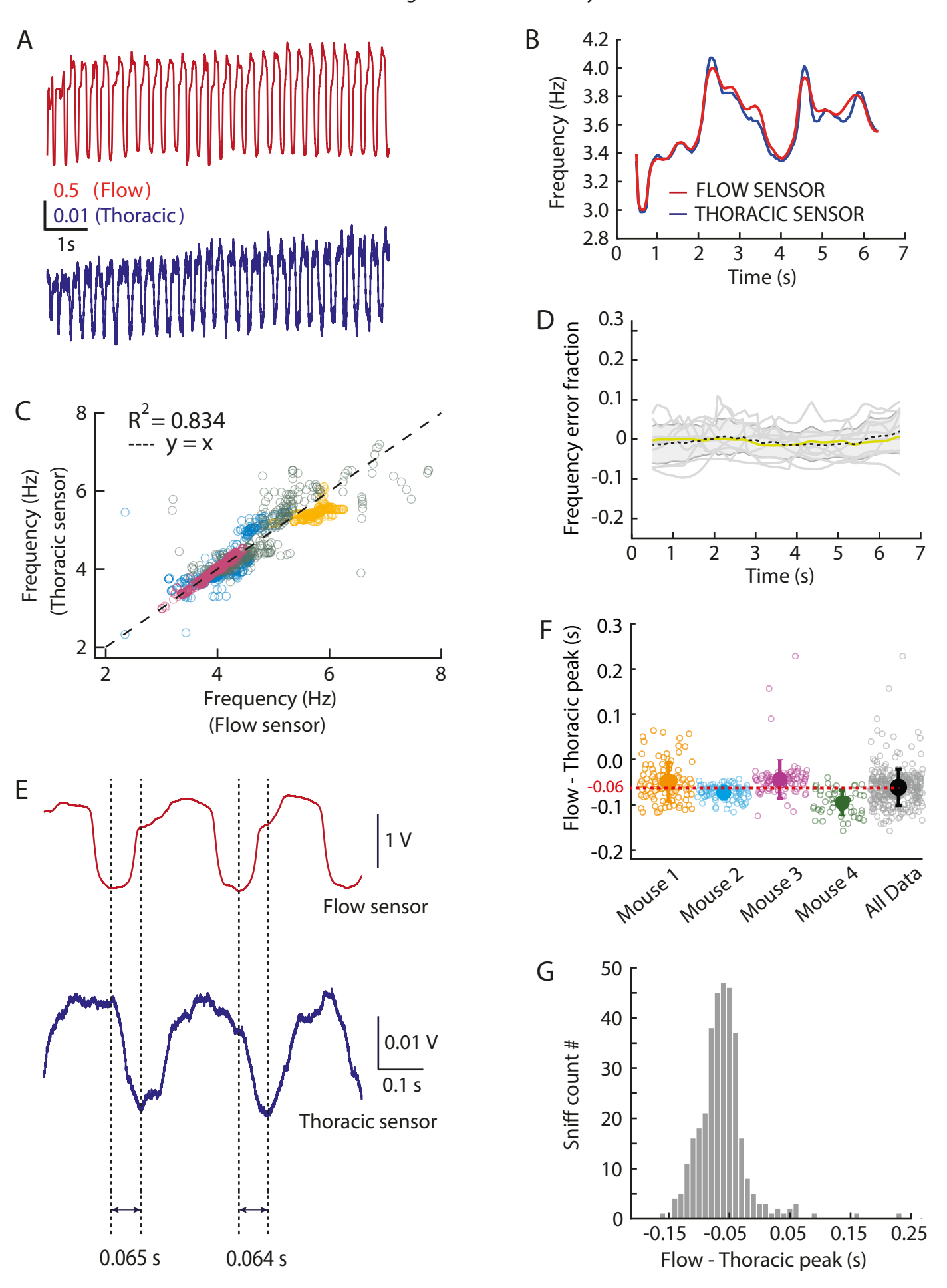


Fig 4. Freely moving schema and analysis

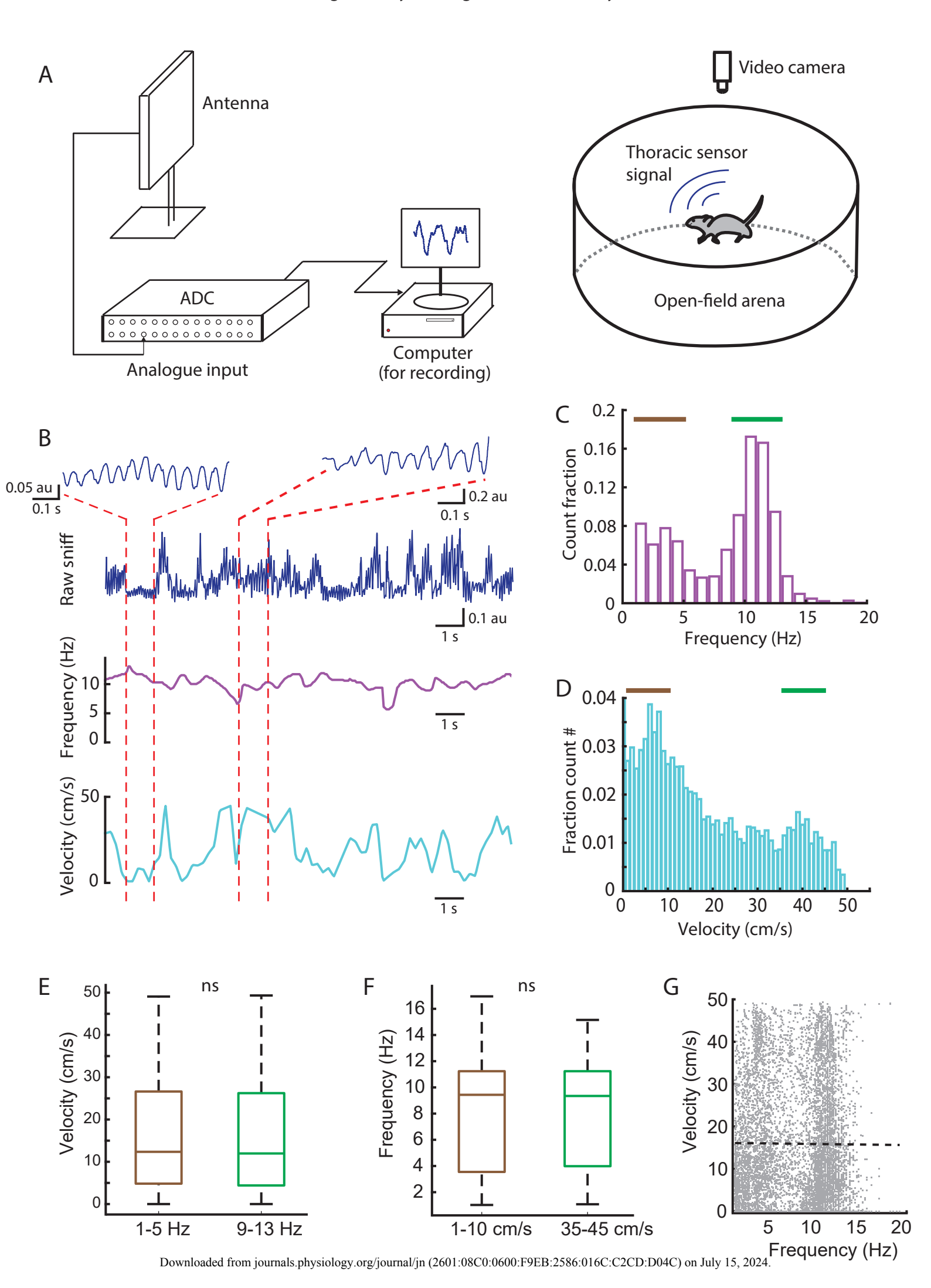
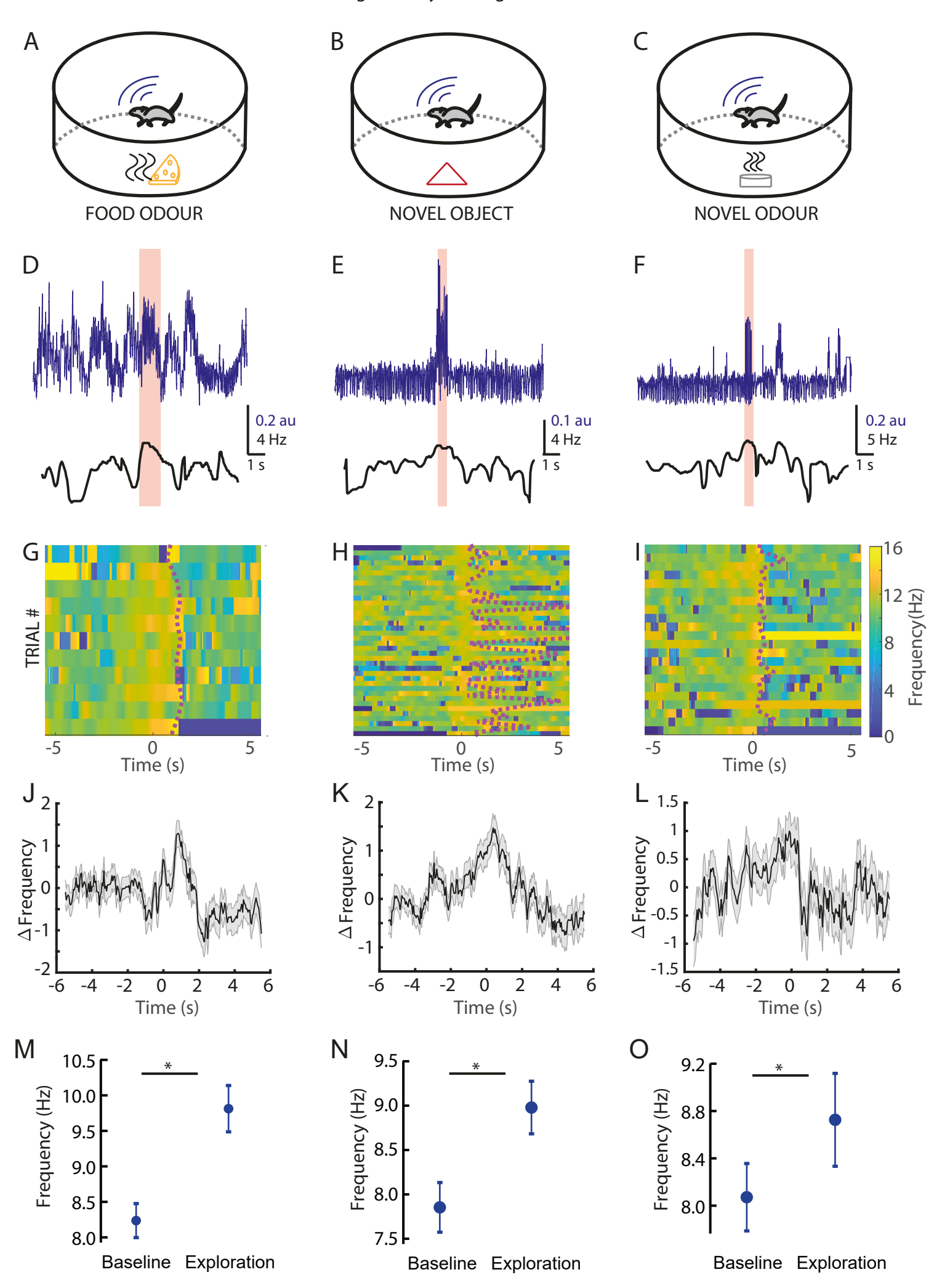


Fig 5. Freely moving Novel cues



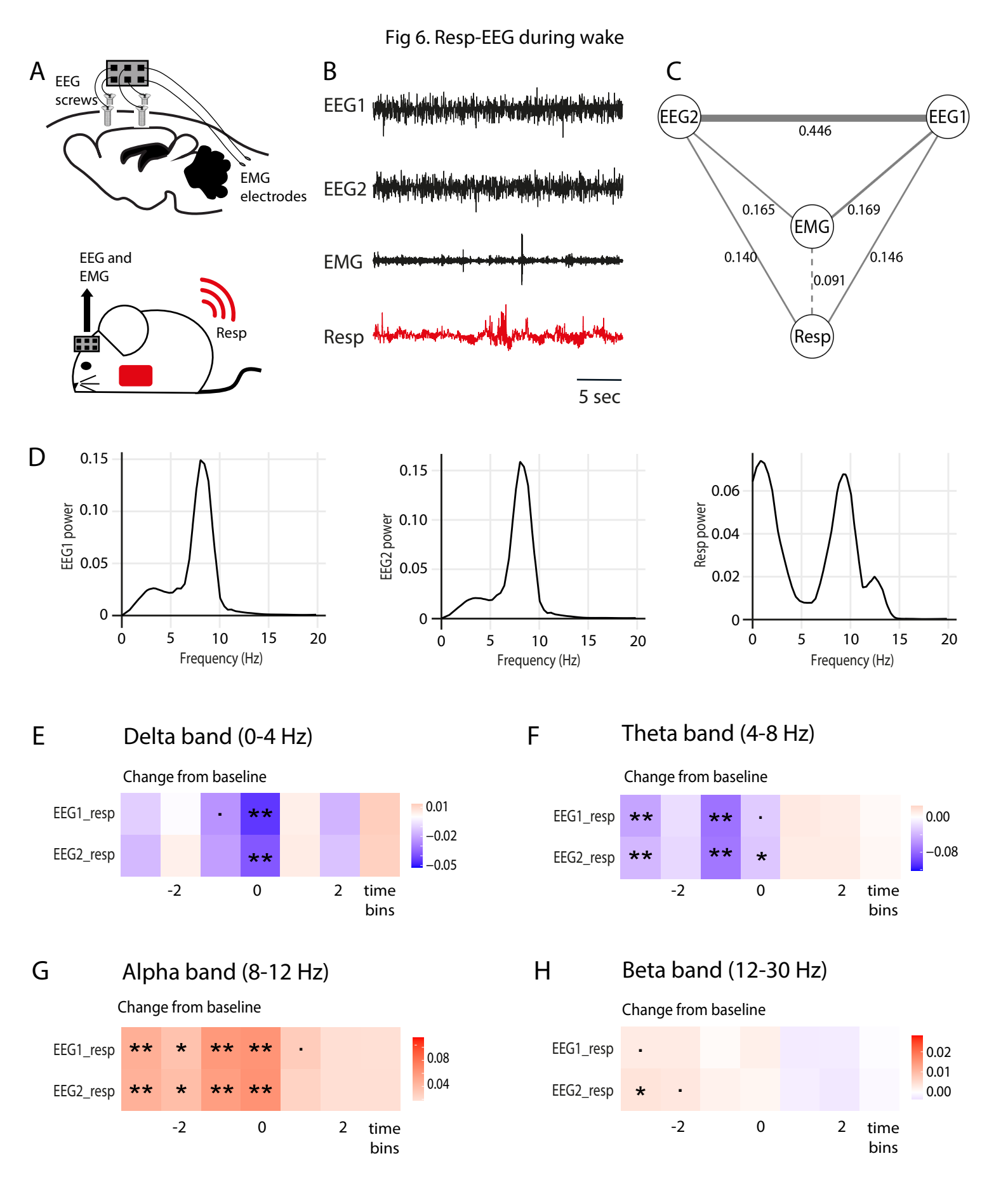


Fig 7. Resp EEG SLEEP

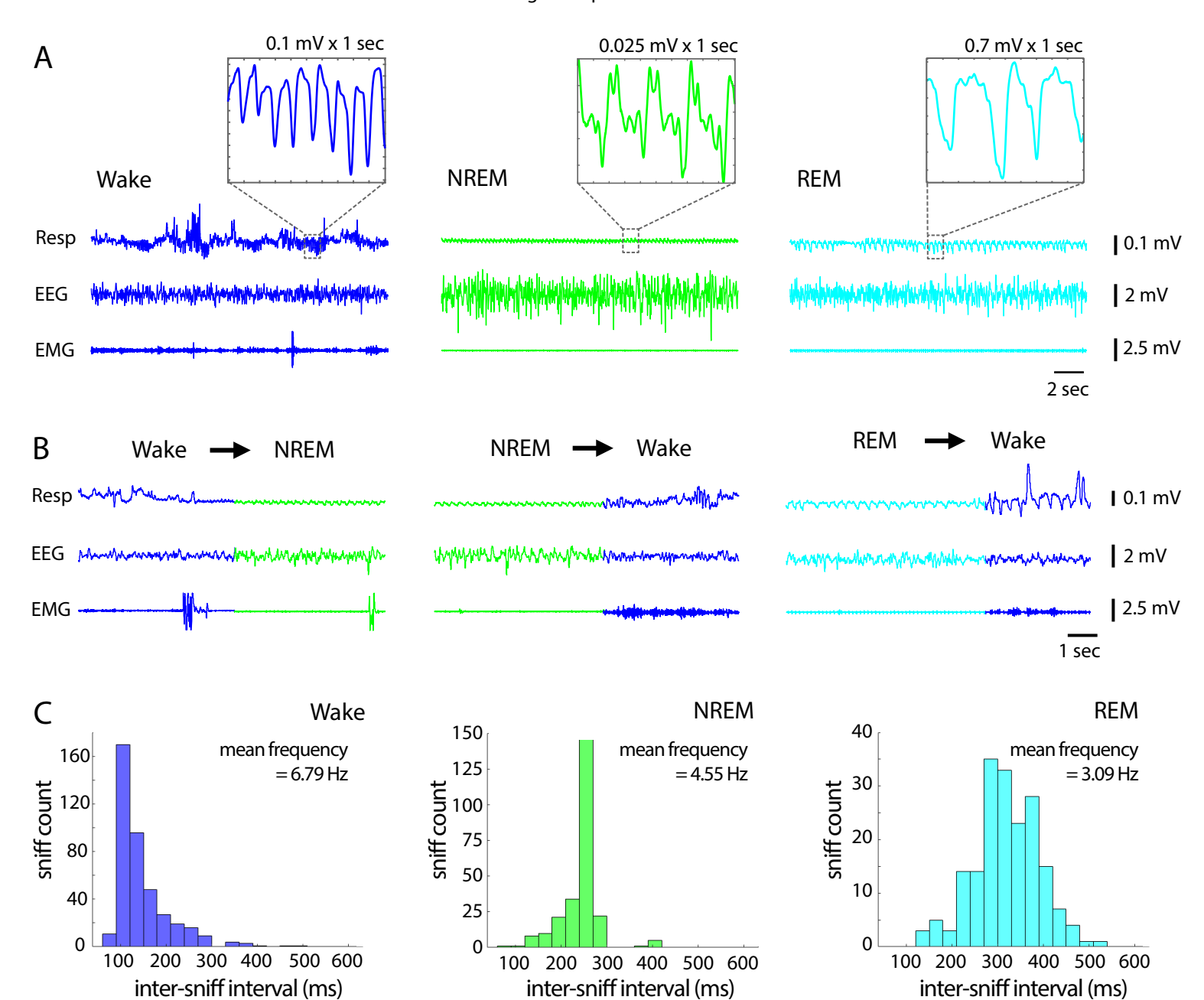


Fig 8. Odour intro sleep Α В state transition detection window **NREM** EEG and wake EMG Resp change analysis windows Resp Resp sensor ON control odour / no odour OFF 0 10 20 30 40 50 -10 odour / no odour C transition to wake transition to REM stayed in NREM Resp NREM REM Wake **EMG** 20 25 30 35 15 20 25 30 35 40 10 15 20 25 30 35 40 10 15 40 10 sec sec sec odour odour odour Η transitions from NREM within 20 seconds Delta Theta % change % change 3% 11% 2 2 stayed 25% 0 in NREM 50% -2 to REM -4 25% 86% -4 -6 10 -6. 10 to Wake 15 20 25 15 20 30 sec odour no odour † odour t odour F Ε G ns resp (Hz) resp (Hz) resp (Hz) resp (Hz) 3 15 15 20 40 10 20 25 30 sec 10 25 30 sec 30 35 50 sec no odour odour control I Delta band (0-4 Hz) Theta band (4-8 Hz) J Change from baseline Change from baseline 0.4 0.50 EEG1_resp EEG1_resp 0.00

EEG2_resp

-2

2

time

bins

0

odour

0.0

EEG2_resp

-2

0

odour

2

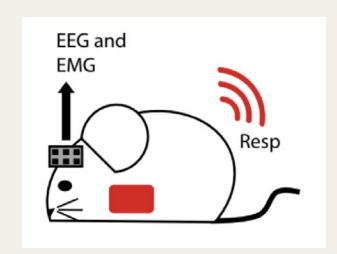
time

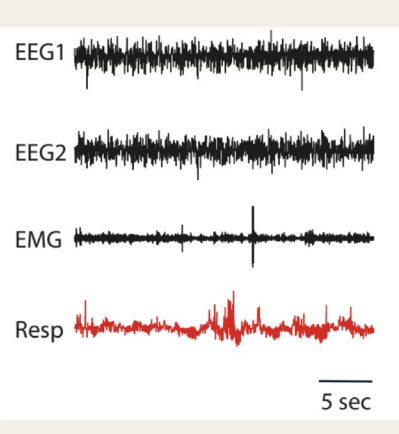
bins

Breathing and Brain Activity across Behavioural States

METHODS

Novel technique to wirelessly monitor respiration

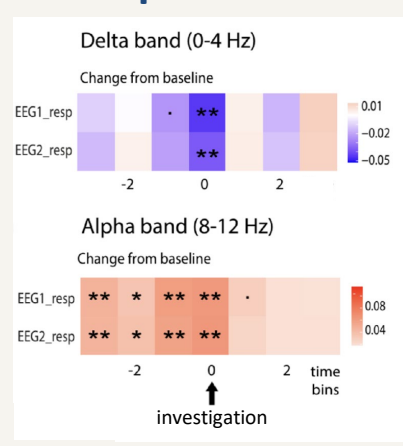




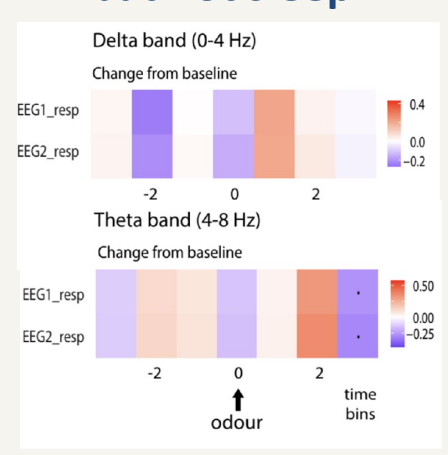
OUTCOME

Specific breathing and brain activity rhythms change their association during:

exploration



but not sleep



CONCLUSION

Wireless respiration monitoring can be combined with brain recording to allow new insights into naturalistic behaviours.